

Acousto-optical metasurfaces for high-resolution acoustic imaging systemsYeonJoon Cheong^{✉*} and Bogdan-Ioan Popa^{✉†}*Department of Mechanical Engineering, University of Michigan, Ann Arbor 48109, USA*

(Received 19 February 2021; revised 23 September 2021; accepted 4 October 2021; published 20 October 2021)

This work introduces a paradigm for acoustic imaging in which a metasurface converts the acoustic waves scattered by remote scenes into coherent light focused into images by conventional optical cameras. The metasurface is composed of acousto-optical unit cells that sense the local acoustic pressure and use the resulting signal to modulate the amplitude of the electric field produced by a laser on an optical aperture. We derive the general design requirements for the image reconstruction in the optical domain and validate the concept through acoustic field measurements of the ultrasound scattered from an object submerged in water followed by numerical simulations predicting how this field is processed by the metasurface and camera. We show that this approach has two main advantages compared to traditional acoustic imaging systems. First, the acoustic-to-optic wavelength down-conversion leads to effective acoustical apertures very large compared to the physical size. Second, the unit cells are not synchronized electronically and thus the complexity of the metasurface increases only linearly with the number of unit cells, which is a significantly slower increase compared to conventional synchronized arrays. This work shows that these advantages lead to compact acoustic cameras providing image resolutions higher than possible with conventional acoustic imaging methods.

DOI: [10.1103/PhysRevB.104.L140304](https://doi.org/10.1103/PhysRevB.104.L140304)

Most acoustic imaging systems such as medical ultrasound scanners and sonar strive to penetrate deeper in the imaged environment while maintaining high resolution. However, diffraction theory stipulates that improving the resolution requires higher-frequency waves, but higher-frequency sound is absorbed at much higher rates than lower frequencies [1] thus reducing penetration depth. One way to maintain low-frequency systems and improve resolution is to increase the aperture of the sensor plane, but conventional acoustic imaging systems have fundamental aperture limitations. They rely on arrays of synchronized transducers. Increasing the number of transducers while keeping them synchronized is a difficult technical challenge and requires cumbersome hardware and large amounts of power [2–5]. For example, the cost per channel of a typical 8-channel data acquisition unit (DAQ) increases by a factor of four compared to a 128-channel DAQ [5]. As a result, the most advanced acoustic imagers have merely tens of thousands of transducers which can only measure sound on apertures less than a hundred wavelengths wide. To put this number in perspective, average commercial optical cameras have sensor containing tens of millions of charge-coupled device (CCD) pixels and are thus tens of thousands of wavelengths in diameter.

A possible way to increase the aperture size is to create optics-inspired systems in which acoustic lenses form an image. This image could be recorded on the acoustic analog of optical CCD sensors, which would employ nonsynchronized transducer elements. The advent of metamaterials have created the means to generate the acoustic lenses [6–12], but

the prototype devices demonstrated so far have very small apertures of several wavelengths, they cannot be tuned in bulk, and they tend to be extremely lossy even at moderate frequencies of several tens of kilohertz [7]. Moreover, there is no acoustic CCD currently available.

This paper explores an alternative imaging paradigm that addresses the limitations of conventional and lens-based acoustic imaging systems. In our approach, acousto-optical metasurfaces (AOM) composed of arrangements of nonsynchronized unit cells convert the acoustic field captured on an acoustic aperture into a coherent optical field presented on an optical aperture. The resulting optical field is focused into an image by off-the-shelf optical cameras. This approach is founded on the observation that radio-to-optical wave conversion in electromagnetic phased array antennas can significantly improve the spatial localization of modern antennas beyond what is possible with traditional techniques [13–15]. More importantly, previous research on down-converting the wavelength of impinging electromagnetic [16,17] and acoustic fields [18,19] and processing the lower wavelength fields has shown a significant increase in resolution due to an effective aperture size larger than its physical size. Consequently, the reduction in wavelength from the millimeter waves of ultrasound acoustics to the submicrometer wavelengths of optics opens the path toward significant improvement of resolution. Finally, our proposed system is not limited by the synchronization-related overhead. Since all the unit cells are completely independent from each other, increasing the aperture requires adding more cells to the system without modifying the existing cells. Thus, the cost and complexity increase linearly with the number of cells, which will likely enable larger apertures than possible with conventional (synchronized) systems.

*yjcheong@umich.edu

†bipopa@umich.edu

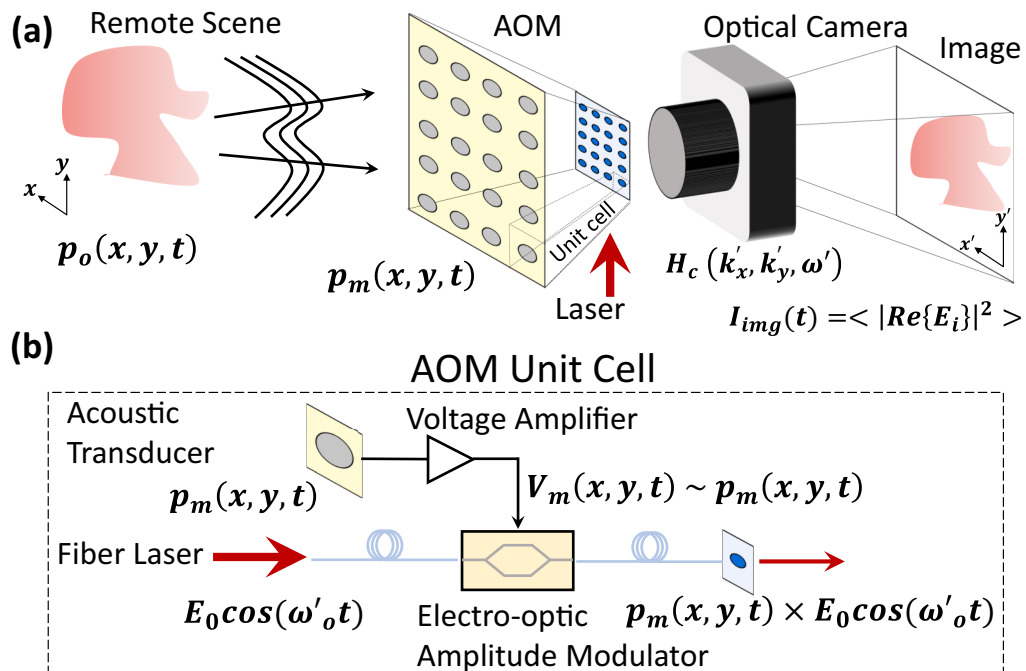


FIG. 1. Acoustic imaging system based on the AOM. (a) The acoustic field scattered by the remote scene p_o is sampled by the acoustical aperture of the metasurface. The sampled field p_m modulates the electric field of a coherent optical field focused into an image by a conventional camera; (b) the acousto-optical unit cell structure.

The AOM physics is explored theoretically and design requirements are derived from this analysis. Furthermore, the concept is demonstrated in experiments in which we measure backscattered echoes from an object submerged in a water tank. We predict the image formation performed by a typical optical camera in numerical simulations to confirm the excellent performance of this approach. Furthermore, we demonstrate the potential of AOM-based imaging systems to break the resolution limit of conventional acoustic imaging systems by showing how they can easily discriminate objects separated by subwavelength distances.

Figure 1(a) presents the design of the proposed acousto-optical system. At the center of the device is the AOM composed of a one-layer periodic arrangement of nonsynchronized independent unit cells. The structure of each unit cell is illustrated in Fig. 1(b) and comprises an acoustic side and an optical side. On the acoustic side, the unit cell senses the local acoustic field scattered by objects in the imaged scene. The resulting electrical signal modulates the amplitude of a laser beam inside an optical modulator. Importantly, all unit cells share the same spatially/temporally coherent laser beam, thus the modulated light produced by all the unit cells on the optical side of the metasurface forms a coherent optical field that contains the amplitude and phase information carried by the impinging sound.

Figure 1(b) shows the possible structure of a unit cell producing the amplitude modulated light wave. The design closely follows a similar radio-frequency-to-light converter cell demonstrated experimentally [14]. In Ref. [14], a radio-frequency (RF) wave was converted into coherent light using an electro-optic modulator and passed through a lens to obtain an image that contains information on the

direction of the impinging RF wave. The electrical signal produced by each RF phased array element was amplified and drove the electro-optic modulator. The resulting intensity-modulated light formed a pixel on the optical aperture. Our unit cells employ a similar idea where the electric signal controlling the modulator comes from an ultrasound transducer instead of an RF antenna element as in Ref. [14].

In our unit cell design, a single laser couples coherent light into a bundle of fibers, each fiber serving one unit cell. An electro-optic modulator such as a lithium niobate modulator [20–23] modifies the electric field amplitude of the impinging light so that the amplitude is proportional to the local acoustic field. For this purpose, the cell is equipped with a piezoelectric transducer that senses the local acoustic pressure. The generated electric signal is amplified and drives the control port of the electro-optic modulator. The output fibers carrying the modulated light from each cell are gathered into an output bundle whose terminations form the optical aperture. In this unit cell design, the minimum back-scattered ultrasound intensity detectable by the acousto-optical metasurface is determined by the sensitivity of the acoustic transducer used to implement the acoustic aperture. Moreover, the quality of the image detected by the CCD camera is determined by other components in the unit cell such as the voltage amplifier, electro-optic modulator, and the sensitivity of the CCD camera. In addition, the amplifier conditions the signal to match the electronic input port requirements of the electro-optic modulators such as dynamic range and impedance. We will show next that this optical field is converted into an accurate representation of the imaged scene by a standard optical camera.

We start by considering the acoustic pressure field scattered by a distant object, p_o , and measured on a plane (called object plane) parallel to the AOM in the object's near-field zone, as shown in Fig. 1(a). Here we assume that the bandwidth of the acoustic field is $2\omega_a$ centered on the angular frequency ω_0 . In this work we follow the convention that the nonprime terms refer to acoustic quantities (e.g., coordinates where acoustical fields are measured, acoustic frequencies, acoustic wave vector components, speed of sound) and the prime quantities refer to optical quantities. Under this convention, the plane-wave decomposition of this field is

$$p_o(x, y, t) = \iiint P_o(k_x, k_y, \omega) e^{j(\omega t - \bar{k}_t \cdot \bar{r}_t)} dk_x dk_y d\omega, \quad (1)$$

where P_o is the three-dimensional (3D) Fourier transform of p_o , $\bar{r}_t = x\hat{x} + y\hat{y}$ is the in-plane (transverse) position vector, \hat{x} , and \hat{y} are unit vectors oriented along the in-plane axes of the Cartesian coordinate system (x, y, z) , and $\bar{k}_t = k_x\hat{x} + k_y\hat{y}$ is the in-plane (transverse) wave vector. Propagating this field a distance z_a away to the acoustic side of the AOM yields the following expression of the acoustic pressure:

$$p_m(x, y, t) = \iiint P_o(k_x, k_y, \omega) e^{j(\omega t - \bar{k} \cdot \bar{r})} dk_x dk_y d\omega, \quad (2)$$

where $\bar{r} = \bar{r}_t + z_a\hat{z}$, \hat{z} is the unit vector oriented along the z axis, $\bar{k} = \bar{k}_t + k_z\hat{z}$, and

$$k_z = \sqrt{\left(\frac{\omega}{c}\right)^2 - k_x^2 - k_y^2}, \quad (3)$$

where c is the speed of sound.

The acoustic field p_m is converted into light using arrays of identical unit cells, whose functionality is sketched in Fig. 1(b). The local field sensed by the unit cell placed at an arbitrary point (x, y) on the acoustical side (aperture) drives an acousto-optical modulator that modulates the amplitude of the electric field $E_0 \cos(\omega_0 t)$ produced by a laser shared by all the unit cells. The modulated optical field is then presented at point (x', y') on the optical side (aperture) of the AOM. We allow the apertures of the acoustical and optical sides. We will see shortly that this requirement is an important design parameter that controls the performance of the AOM. From a practical point of view, this difference in sizes is also warranted because of the large contrast between the size of the acoustical transducer (which can be a piezoelectric element or a microphone) and the size of the driven optical element on the optical side (which can be the end of an optical fiber). We define the aperture scaling factor η so that the sensed local field at the point of coordinates (x, y) on the acoustical side modulates the optical output of the cell at coordinates (x', y') according to the mapping $x' = \eta x$ and $y' = \eta y$. With this notation and considering the electro-optic amplitude modulation in the unit cells [see Fig. 1(b)], the electrical field on the optical aperture is the real part of [20,24]

$$E_m(x', y', t) = E_0 e^{j\omega_0 t} p_m(x, y, t). \quad (4)$$

We plug p_m given by Eq. (2) in the latter expression and use the change of variables $k'_x = k_x \eta^{-1}$, $k'_y = k_y \eta^{-1}$, and

$\omega' = \omega'_0 + \omega$ to obtain

$$E_m = E_0 \eta^2 \iiint P_o(\eta k'_x, \eta k'_y, \omega' - \omega'_0) e^{-jk_z z_a} \times e^{j(\omega' t - k'_x x' - k'_y y')} dk'_x dk'_y d\omega'. \quad (5)$$

This equation is remarkable because it corresponds to the optical field scattered by an object whose optical spatial-temporal spectrum P_o is identical to that of the original scene and which is situated a distance $z_l = k_z z_a / k'_z$ away from the optical aperture, where $k'_z = \sqrt{k'^2 - k'^2_x - k'^2_y}$ and $k' = \omega' / c'$ is the optical wave number. This is strong indication that an optical camera could produce an optical image of this object, which is demonstrated next.

To quantify the effect of the camera on the optical field E_m , we consider its coherent optical transfer function $H(k'_x, k'_y, \omega')$ when the camera is tuned to image objects situated z_l away from its input aperture. This transfer function has two components, i.e., $H(k'_x, k'_y, \omega') = H_f(k'_x, k'_y, \omega') H_c(k'_x, k'_y, \omega')$. The first, $H_f(k'_x, k'_y, \omega') = e^{-jz_l k'_z}$, represents the free-space propagation of the spectral component (i.e., plane wave) having the angular frequency ω' and the transverse wave vector components k'_x and k'_y over the distance z_l between the object and the camera's input aperture. The second corresponds to the propagation of this spectral component through the lens elements to the optical sensor. It follows that $H_c(k'_x, k'_y, \omega') = H(k'_x, k'_y, \omega') e^{jz_l k'_z}$. Consequently, propagating E_m to the image plane at the camera's sensor yields an electric field component $E_i(x', y', t)$ given by

$$E_i = E_0 \eta^2 \iiint P_o(\eta k'_x, \eta k'_y, \omega' - \omega'_0) H(k'_x, k'_y, \omega') \times e^{j(\omega' t - k'_x x' - k'_y y')} e^{j\phi} dk'_x dk'_y d\omega', \quad (6)$$

where

$$\phi = -z_a k_z + z_l k'_z. \quad (7)$$

If we can design the acousto-optical system so that it has constant $\phi \approx \phi_0$ then Eq. (6) becomes

$$E_i = E_0 \eta^2 \tilde{p}_o(x', y', t) e^{j\phi_0}, \quad (8)$$

where

$$\tilde{p}_o(x', y', t) = \iiint P_o(\eta k'_x, \eta k'_y, \omega' - \omega'_0) H(k'_x, k'_y, \omega') \times e^{j(\omega' t - k'_x x' - k'_y y')} dk'_x dk'_y d\omega' \quad (9)$$

represents the optical image through the camera of an object \tilde{p}_o whose spatial spectral components P_o are identical to the spectral components of the original scene. This remarkable result means that we obtain an accurate optical image of the remote scene shown in Fig. 1 which was probed acoustically.

Equation (8) provides another important physical insight into the operation of the acousto-optical camera presented in Fig. 1. The optical intensity measured by the camera is the time average $I_{\text{img}} = \langle |\text{Re}\{E_i\}|^2 \rangle$. The averaging interval is large comparable to the optical period $2\pi / \omega'$ but orders of magnitude smaller than the acoustic period $2\pi / \omega$. Therefore, the intensity at the camera CCD sensor and thus the image

becomes

$$I_{\text{img}}(t) = \frac{(E_0 \eta^2)^2}{2} \tilde{p}_o^2(x', y', t). \quad (10)$$

This equation means that a high-speed camera could produce a series of snapshots of the acoustic field measured on planes situated progressively farther away at distances $d = ct$. Consequently, the proposed imaging system can provide the entire 3D distribution of the acoustic field in front of the AOM.

The image reconstructions predicted by Eq. (10) is accurate when the parameter ϕ given by Eq. (7) is constant with respect to the transverse wave number defined as $k_t'^2 = k_x'^2 + k_y'^2$ and the optical angular frequency $\omega' \approx \omega'_0$. It is thus in order to discuss the effect of the design parameters on the value of ϕ .

The parameters controlled in the design process are the ratio of optical-to-acoustic aperture diameters (η), the optimum object distance for which the image produced by the camera is sharpest (z_l), the bandwidth of the acoustic wave ($2\omega_a$), and the ratio between the acoustic and optic wavelengths ($\epsilon = \lambda'_0/\lambda_0$).

We expand the expression of ϕ by taking into account the definitions of k_z and k'_z provided earlier to obtain

$$\phi = z_l \sqrt{\left(\frac{\omega'_0}{c'}\right)^2 - k_t'^2} - z_a \eta \sqrt{\left(\frac{\omega}{\eta c}\right)^2 - k_t'^2}. \quad (11)$$

This equation shows that constant ϕ could easily be obtained when the acoustic scene is ensonified with monotone ultrasound, i.e., $\omega_a = 0$ and $\omega = \omega_0$. In this scenario, using the Fresnel approximation when $k_t'^2 = k_x'^2 + k_y'^2 \ll k_0'^2$ and $\eta^2 k_t'^2 = k_x^2 + k_y^2 \ll \omega_0^2/c^2$ we can simplify Eq. (11) to the following expression:

$$\phi = k_0' z_l - k_0' \epsilon z_a + \frac{k_t'^2}{2k_0'} \left(z_l - z_a \frac{\eta^2}{\epsilon} \right). \quad (12)$$

Therefore, ϕ is constant when we choose

$$z_l = z_a \frac{\eta^2}{\epsilon}. \quad (13)$$

Most acoustical imaging systems such as medical ultrasound imagers and sonar devices use short pulses that have nonzero bandwidths. Assuming that the bandwidth is $2\omega_a$, the second term of Eq. (11) will vary with the acoustic frequency $\omega \in (\omega_0 - \omega_a, \omega_0 + \omega_a)$ and thus ϕ will also vary with frequency, which leads to distortions in the final image. However, the following proof of concept experiment shows that excellent imaging performance is maintained when we limit the ϕ swing below 45° for all $k_t' \ll k_0'$ and ω .

To illustrate the acousto-optical camera concept, we performed the experiment shown in Fig. 2. An object (letter M) was submerged into a water tank and ensonified using an omnidirectional hydrophone (Teledyne-Reson TC 4013) placed 25 cm away from the object as shown in Fig. 2(a). The temporal spectrum of the acoustic pulse launched by the hydrophone has a center frequency of $f_0 = \omega_0/2\pi = 100$ kHz and a 3-dB bandwidth of $2\omega_a/2\pi = 30$ kHz [see Fig. 2(b)]. Using the method described in Ref. [25], the acoustic field scattered by the object is measured by a second hydrophone that raster scans an area of 405 mm by 345 mm parallel to the object and situated at a distance $z_a = 0.25$ m away from

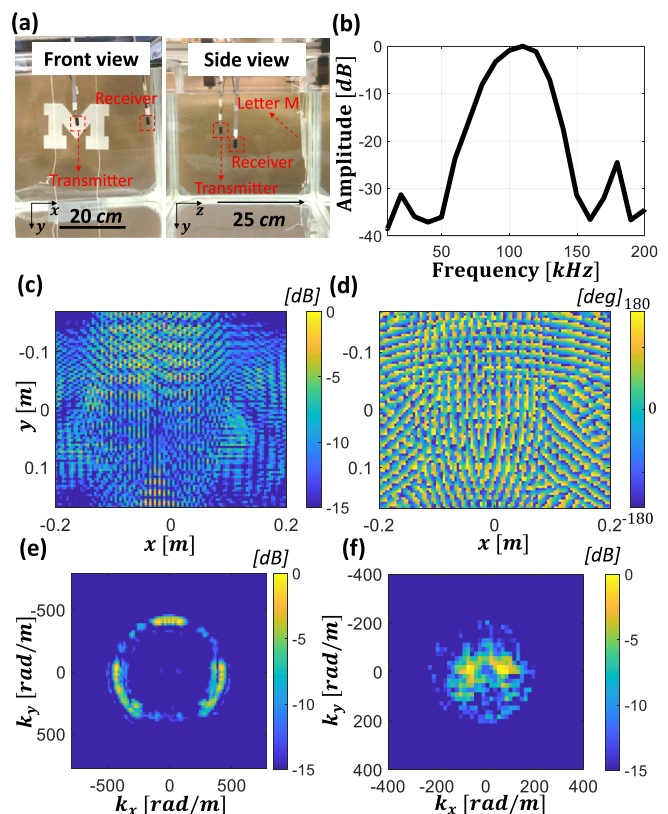


FIG. 2. Acoustic field measurements. (a) Underwater acoustic field measurement setup with object (letter M) placed $z_a = 0.25$ m from the measurement plane. (b) Spectrum of the transmitted acoustic signal centered at 100 kHz with -3 dB bandwidth of 30 kHz. [(c) and (d)] The intensity and the phase of measured field at 100 kHz. (e) The measured field intensity $|P_m|^2$ in k space at 100 kHz shows the reverberant nature of the water tank. (f) Same as (e) after applying a spatial low pass filter to keep only the components $\sqrt{k_x^2 + k_y^2} < k_0/2$, where $k_0 = \omega_0/c = 418$ m^{-1} . The intensity at (f) is renormalized with respect to the largest value.

the object. This measurement replicates the acoustic pressure field sampled by the unit cells on the acoustical side of the AOM. The scanning is done in steps of 4 mm to simulate a AOM unit cell periodicity of 4 mm.

Figures 2(c) and 2(d) show the intensity and phase of the measured acoustic pressure at 100 kHz. The k -space amplitude of the pressure field $|P_m(k_x, k_y, \omega_0)|$ is presented in Fig. 2(e) and shows that the measured pressure field contains not only the echoes from the object but also reflections of the impinging ultrasound pulses from the water tank walls. We filter out the latter by removing all the transverse wave numbers larger than 209 rad/m, which correspond to plane waves reflected by the water tank walls and propagating at steep angle relative to the normal to the object. Figure 2(f) shows the remaining plane-wave components dominated by the reflections from the object.

To demonstrate the image formation of the letter M through the AOM-based camera, we simulate numerically the effect of the acousto-optical metamaterial and the propagation of the ensuing optical field to the camera's CCD sensor using Eqs. (4)–(10). In these simulations we assume a laser wavelength $\lambda'_0 = 532$ nm and we choose $\eta = 10^{-2}$, which

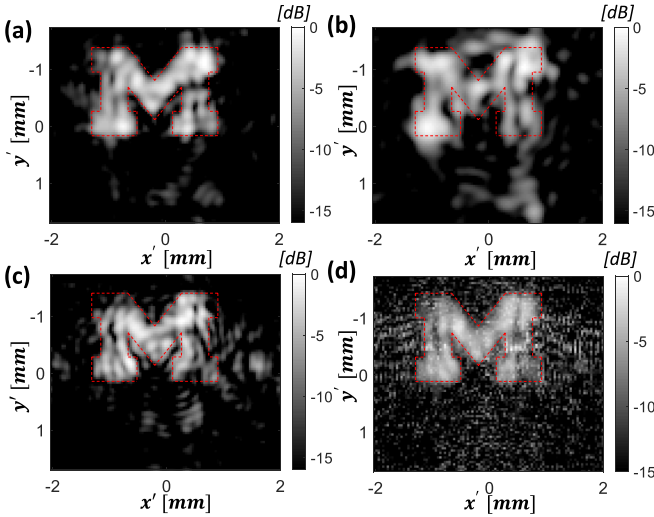


FIG. 3. The optical intensity of the reconstructed image field when the scene is probed with monotone ultrasound at (a) 100 kHz, (b) 75 kHz, and (c) 125 kHz. (d) Image representing the optical intensity when the scene is probed with a broadband pulse centered at 100 kHz and having a 3-dB bandwidth of 30 kHz.

corresponds to an optical aperture of the AOM of approximately $4 \text{ mm} \times 4 \text{ mm}$. It follows that $\epsilon = \lambda'_0/\lambda_0 = 3.5 \times 10^{-5}$ and $z_l = 0.70 \text{ m}$ as given by Eq. (13). In principle, any optical camera could be used to focus the optical field on the AOM optical aperture into an image. For ease of calculation of the camera's optical transfer function, we choose a simple yet effective 4F camera [26] consisting of two lenses of focal length z_l placed in the focal plane of each other. The AOM optical aperture is placed against the first lens and the CCD sensor is placed on the focal plane of the second lens.

Figure 3 shows the images recovered at the image plane using Eq. (10) in four scenarios. Figures 3(a)–3(c) show the images when monotonic acoustic waves were used at the frequencies 100, 75, and 125 kHz, respectively. Specifically, the results were obtained from a single broadband measurement using the acoustic pulse shown in Fig. 2(b) and assuming harmonic acoustic waves at these frequencies were used to drive the AOM. A very good image was obtained at the design frequency of 100 kHz as illustrated by Fig. 3(a).

Away from the design frequency, the images are degraded because ϕ given by Eq. (7) varies with the transverse wave number k'_t and with the frequency. Equation (11) quantifies the variation of ϕ versus design parameters, which allows us to design imaging systems for which ϕ is small even for broadband impinging waves. For example, in the example shown in Fig. 2, ϕ has a swing of up to 45° at 75 and 125 kHz, but the images maintain good quality as seen in Figs. 3(b) and 3(c). Figure 3(d) shows the image formation when we take into account the entire bandwidth of the acoustic pulse used in the experiment. The figure demonstrates an accurate image formation of the letter M despite the adverse effect of the nonconstant ϕ .

Past research [16–19] has shown that down-converting the wavelength of the probing waves in an imaging system generally leads to higher resolutions than it is possible in conventional systems because the ratio aperture-to-wavelength

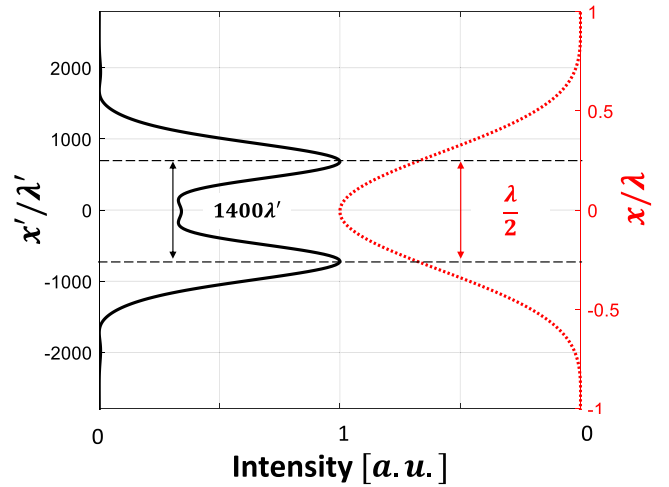


FIG. 4. The recovered images of two point sources using the AOM camera (left) and the conventional method (right). The former is able to resolve the two scatterers, and the latter fails.

increases in the former cases. This has been demonstrated in systems that down-convert the wavelength by a factor of two or three. We show in the following that this effect is dramatic for the AOM-based camera that down-converts the wavelength by several orders of magnitude.

Diffraction theory [24,26] defines the resolution limit as the separation between two points sources for which the two sources are indistinguishable in the far field. Typically used criteria such as Rayleigh and Sparrow limits quantify this separation to $\sim \lambda/2$. We consider a simulated scenario with two point sources emitting harmonic spherical acoustic waves at the frequency $f_0 = 1000 \text{ Hz}$. The scatterers are separated by $\lambda_0/2$ and therefore a traditional linear acoustic imaging system would not be able to discriminate their positions. The fields are sensed on a square aperture of side $A = 2.5 \text{ m}$ situated $z_a = 0.15 \text{ m}$ away from the sources and pass through an ideal lens-based linear acoustic imaging system having the acoustic transfer function [26]

$$H(k_x, k_y) = P\left(\lambda_0 z_i \frac{k_x}{2\pi}, \lambda_0 z_i \frac{k_y}{2\pi}\right), \quad (14)$$

where z_i is the distance between the exit of the lens system and the image plane of the system, and the pupil function $P(x, y) = 1$ inside the aperture (i.e., for $-A/2 < x < A/2$ and $-A/2 < y < A/2$) and is zero otherwise. The reconstructed image through this system is illustrated in Fig. 4 (dotted curve). As diffraction theory predicts, the intensity in the image plane shows only one maximum, which makes the scatterer discrimination impossible.

In contrast, the AOM is able to clearly differentiate the scatterers as shown by the left curve in Fig. 4. In simulating the acousto-optical metasurface imaging system, we considered 500×500 unit cells covering the square aperture of side 2.5 m . The number of unit cells is not particularly important here as long as the cell lattice periodicity is at most half of the transverse wavelength in the acoustic aperture. The design parameters used in the simulation are $\lambda'_0 = 532 \text{ nm}$, $z_a = 0.15 \text{ m}$, and $\eta = 10^{-3}$ and thus $\epsilon = 3.5 \times 10^{-7}$ and $z_l = 0.41 \text{ m}$. In this case the scatterer separation is three orders

of magnitude larger than the wavelength used to create the image.

To conclude, this work introduced an acoustic imaging paradigm in which the scattered acoustic field is converted into an optical field by an acousto-optical metasurface. The metasurface is composed of independent unit cells that modulate the light amplitude of a coherent light source. Analytical equations based on the plane-wave decomposition of the resulting optical field provided the design constraints of the AOM and showed that the optical field can be focused into an image by off-the-shelf commercial cameras. We demonstrated the concept using a hybrid approach in which we measured the acoustic field scattered by an object and simulated the action of the AOM-based device. This proof of concept illustration confirmed the effectiveness of our method. The hardware needed to implement the proposed metasurface already exists and has been experimentally demonstrated in a different application, i.e., visualizing the direction of impinging RF waves.

In our approach the image formation is done in the physical space by the optical camera as opposed to using a

computer. This removes the need to synchronize electronically the unit cells composing the metasurface. This is an essential departure from traditional acoustic imaging systems such as medical ultrasound machines or sonar that require the electronic synchronization of arrays of transducers and thus can only have a limited number of transducers. In contrast, the number of AOM unit cells can be increased significantly compared to traditional systems, which will lead to higher resolution systems.

The acoustic-to-optic wavelength down-conversion is another source of resolution enhancement. The enhancement is due to the effective optical aperture used during the optical image reconstruction being significantly larger than the physical acoustic aperture by a factor of η/ϵ . This is a remarkable property that will enable imaging systems that produce high resolution images even when low-frequency probing sound is employed.

This material is based on work supported by the National Science Foundation under Grant No. CMMI-1942901.

-
- [1] C. R. Hill, J. C. Bamber, and G. R. ter Haar, *Physical Principles of Medical Ultrasonics*, 2nd ed. (John Wiley & Sons, New York, 2004).
- [2] A. Izquierdo, J. J. Villacorta, L. Del Val, L. Suárez, and D. Suárez, *Sensors* **18**, 25 (2018).
- [3] B. Da Silva, A. Braeken, and A. Touhafi, *Computers* **7**, 41 (2018).
- [4] A. Izquierdo, J. J. Villacorta, L. del Val Puente, and L. Suárez, *Sensors* **16**, 1671 (2016).
- [5] A. Fatima, K. Kratkiewicz, R. Manwar, M. Zafar, R. Zhang, B. Huang, N. Dadashzadeh, J. Xia, and K. M. Avanaki, *Photoacoustics* **15**, 100137 (2019).
- [6] A. Climente, D. Torrent, and J. Sanchez-Dehesa, *Appl. Phys. Lett.* **97**, 104103 (2010).
- [7] T. P. Martin, M. Nicholas, G. J. Orris, L.-W. Cai, D. Torrent, and J. Sanchez-Dehesa, *Appl. Phys. Lett.* **97**, 113503 (2010).
- [8] L. Zigoneanu, B.-I. Popa, and S. A. Cummer, *Phys. Rev. B* **84**, 024305 (2011).
- [9] G. Grelowska and E. Kozaczka, *Arch. Acoust.* **39**, 439 (2014).
- [10] V. Pallayil, M. Chitre, S. Kuselan, A. Raichur, M. Ignatius, and J. R. Potter, *IEEE J. Ocean. Eng.* **41**, 175 (2016).
- [11] Y. Xie, C. Shen, W. Wang, J. Li, D. Suo, B.-I. Popa, Y. Jing, and S. A. Cummer, *Sci. Rep.* **6**, 35437 (2016).
- [12] Y. Tian, Q. Wei, Y. Cheng, and X. Liu, *Appl. Phys. Lett.* **110**, 191901 (2017).
- [13] J. Macario, P. Yao, S. Shi, A. Zabolckj, C. Harrity, R. D. Martin, C. A. Schuetz, and D. W. Prather, *Opt. Express* **20**, 23623 (2012).
- [14] J. Murakowski, G. J. Schneider, S. Shi, C. A. Schuetz, and D. W. Prather, *Opt. Express* **25**, 15746 (2017).
- [15] D. W. Prather, S. Shi, G. J. Schneider, P. Yao, C. Schuetz, J. Murakowski, J. C. Deroba, F. Wang, M. R. Konkol, and D. D. Ross, *IEEE Trans. Antenn. Propag.* **65**, 6432 (2017).
- [16] Z. Wang, Y. Luo, T. Jiang, Z. Wang, J. Huangfu, and L. Ran, *Phys. Rev. Lett.* **106**, 047402 (2011).
- [17] Y. Cheong, K. A. Shorter, and B.-I. Popa, *IEEE Antenn. Wirel. Propag. Lett.* **18**, 118 (2018).
- [18] B.-I. Popa, D. Shinde, A. Konneker, and S. A. Cummer, *Phys. Rev. B* **91**, 220303(R) (2015).
- [19] Y. Cheong, K. A. Shorter, and B.-I. Popa, *Appl. Acoust.* **174**, 107800 (2021).
- [20] J. Capmany and C. R. Fernández-Pousa, *Laser Photon. Rev.* **5**, 750 (2011).
- [21] A. Rao and S. Fathpour, *IEEE J. Sel. Top. Quant. Electron.* **24**, 4 (2017).
- [22] C. Wang, M. Zhang, X. Chen, M. Bertrand, A. Shams-Ansari, S. Chandrasekhar, P. Winzer, and M. Lončar, *Nature (Lond.)* **562**, 101 (2018).
- [23] C. Wang, M. Zhang, B. Stern, M. Lipson, and M. Lončar, *Opt. Express* **26**, 1547 (2018).
- [24] B. E. Saleh and M. C. Teich, *Fundamentals of Photonics* (John Wiley & Sons, New York, 2019).
- [25] B.-I. Popa, W. Wang, A. Konneker, S. A. Cummer, C. A. Rohde, T. P. Martin, G. J. Orris, and M. D. Guild, *J. Acoust. Soc. Am.* **139**, 3325 (2016).
- [26] J. W. Goodman, *Introduction to Fourier Optics* (Roberts & Company Publishers, Greenwood Village, CO, 2005).